Physica D 70 (1994) 370–382
North-Holland

SSDI: 0167-2789(93)E0291-I

PHYSICA D

Irregular wakes in reaction–diffusion waves

Jonathan A. Sherratt
Centre for Mathematical Biology, Mathematical Institute, 24-29 St. Giles', Oxford OX1 3LB, UK
and Nonlinear Systems Laboratory, Mathematics Institute, University of Warwick, Coventry CV4 7AL, UK

Received 9 October 1992
Revised manuscript received 20 June 1993
Accepted 20 September 1993
Communicated by A.V. Holden

Reaction–diffusion equations have proved to be highly successful models for a wide range of biological and chemical systems, but chaotic solutions have been very rarely documented. We present a new mechanism for generating apparently chaotic spatiotemporal irregularity in such systems, by analysing in detail the bifurcation structure of a particular set of reaction–diffusion equations on an infinite one-dimensional domain, with particular initial conditions. We show that possible solutions include travelling fronts which leave behind either regular or irregular spatiotemporal oscillations. Using a combination of analytical and numerical analysis, we show that the irregular behaviour arises from the instability of oscillations induced by the passage of the front. Finally, we discuss the generality of this mechanism as a way in which spatiotemporal irregularities can arise naturally in reaction–diffusion systems.

1. Introduction

Reaction–diffusion equations have proved to be highly successful models for a wide range of biological and chemical systems. The most celebrated applications include the evolution of spatial pattern in developmental biology [1–3], the movement of travelling fronts of cells, animal herds and reacting chemicals [4–6], and the propagation of spiral waves in chemical systems such as the Belousov–Zhabotinskii reaction [7–9]. In view of this wide range of nonlinear phenomena captured by these models, it is perhaps a little surprising that spatiotemporal chaos has been so rarely documented. A number of authors have investigated chaotic solutions in systems of two or more oscillators with diffusive-type coupling (see below), but chaotic solutions of partial differential equations of reaction–diffusion type have previously been restricted mainly to the hypothetical trimolecular reaction known as the 'Brussellator' [10]. When the diffusion coefficients are sufficiently different in this system, spatially homogeneous oscillations, which correspond to a limit cycle solution of the kinetics, are unstable to nonuniform perturbations, and the system evolves to spatiotemporal chaos [11–13].

This rarity of chaotic solutions of reaction–diffusion equations is in marked contrast to spatially discrete systems. A wide range of cellular automata exhibit spatiotemporal chaos [14], including models for species interactions [15–17], chemical reactions [18–20], and fluid dynamics [21]. Moreover, systems of oscillators coupled by linear transport often exhibit chaotic solutions. These systems typically have the form

$$\begin{aligned}\dot{u}_{i,j} = {} & F_i(u_{i,j}, \ldots, u_{I,j}) \\ & + D_i(u_{i,j+1} - u_{i,j}) \cdot \mathcal{I}[j \neq J] \\ & + D_i(u_{i,j} - u_{i,j-1}) \cdot \mathcal{I}[j \neq 1] \end{aligned} \tag{1}$$

$(1 \leq i \leq I,\ 1 \leq j \leq J)$, which is J copies of the Ith order system $\dot{\boldsymbol{\zeta}} = \boldsymbol{F}(\boldsymbol{\zeta})$, with linear coupling between adjacent copies; here $\mathcal{I}$ denotes the logical function, with $\mathcal{I}[.\text{TRUE.}] = 1$ and $\mathcal{I}[.\text{FALSE.}] = 0$. A number of authors have shown, for various systems, that if $\dot{\boldsymbol{\zeta}} = \boldsymbol{F}(\boldsymbol{\zeta})$ has a limit cycle solution then (1) may possess chaotic solutions [22–25], while if $\dot{\boldsymbol{\zeta}} = \boldsymbol{F}(\boldsymbol{\zeta})$ itself exhibits chaos, the coupling can induce non-uniform chaos [26].

In this paper, we discuss a new mechanism by which irregular spatiotemporal oscillations arise naturally in a particular system of two coupled reaction–diffusion equations. We have not attempted numerical calculation of the Lyapunov exponents, or other numerical tests for chaos, and thus we avoid using the word "chaos" to describe our results. The behaviour we will discuss is quite different from that in the Brussellator [11–13], since the irregular behaviour arises even when the two diffusion coefficients are the same. We go on to discuss the generality of our results as mechanism for generating spatiotemporal irregularity in reaction–diffusion systems.

2. The model equations

The density of cells in mammalian tissue is maintained in a dynamic equilibrium, with cell division balancing natural cell death. In order to maintain this equilibrium, cell proliferation is carefully controlled. In addition to the direct effects of crowding as a check on growth, cells secrete a number of regulatory biochemicals, which either stimulate or inhibit their own division. This complex control mechanism enables cell proliferation to increase rapidly when necessary, for instance during wound healing [27–29]. However, genetic mutations can give rise to cells which exploit these biochemical control mechanisms to gain a proliferative advantage over normal cells; this type of mutation is a key aspect of carcinogenesis [30,31]. Two possible effects of such a mutation are decreased production of an auto-inhibitor of cell division, and decreased response to such an inhibitor. To model this process mathematically, we suppose that cells produce the inhibitory chemical at a constant rate, which is h, say, for the normal cells, and $P \cdot h$ $(P < 1)$ for the mutant cells. This production is balanced by a corresponding rate of chemical decay. We can reasonably assume that the chemical kinetics are very fast compared with cell division [32,33], so that the chemical concentration is approximately proportional to $n + Pm$, where $n(x,t)$ and $m(x,t)$ are the local densities of normal and mutant cells respectively. Here x and t denote space and time; for simplicity we consider only the case of one space dimension. We therefore expect that after appropriate nondimensionalization [33] the conservation equations for normal and mutant cells will have the following form:

$$\frac{\partial n}{\partial t} = D\frac{\partial^2 n}{\partial x^2} + n[f(n+m)g(n+Pm) - 1], \tag{2a}$$

$$\frac{\partial m}{\partial t} = D\frac{\partial^2 m}{\partial x^2} + m[f(n+m)g(\xi n + \xi P m) - \gamma]. \tag{2b}$$

Here $f(n+m)$ represents the effect of crowding on cell division, and $g(n+Pm)$ represents the auto-inhibition; f and g are both decreasing functions. The constant ξ (< 1) represents the decreased response of the mutant cells to the inhibitor, while the positive constant γ is greater than 1, corresponding to an increased death rate of mutant cells due to an immune response [34]. To ensure that, following our nondimensionalisation, the normal state $n = 1$, $m = 0$ is an equilibrium, we impose the conditions $f(1) = g(1) = 1$, and we take simple functional forms satisfying these criteria, namely $f(\zeta) = (N - \zeta)/(N-1)$ and $g(\zeta) = k/[1 + (k-1)\zeta]$. Here N and k are constants, both greater than 1; N is

an upper limit on the total cell density, due to crowding. Following a number of previous authors [27,35,36], we represent cell movement by linear diffusion, which is valid provided the cell density in the tissue is not too large.

We have previously discussed in detail the solution of (2) when the equilibrium $n = 1$, $m = 0$ is given a small localized perturbation, for parameters satisfying $1 > P > 0$, $\xi < 1$ and $\gamma > 1$ [33,37]. In particular, we have shown that the equilibrium is stable to such perturbations if $\gamma > g(\xi)$, and that otherwise a travelling front moves outwards from the site of the perturbation, leaving the system in a steady state with $m \neq 0$. The front speed is given approximately by $2\sqrt{D[g(\xi) - \gamma]} \equiv a$, say, which is independent of the parameter P; however, the solution behind the travelling front depends crucially on P. For P close to 1, the system is in the steady state $n = 0$, $m = M$ behind the front, where M is the unique root on $(1, \infty)$ of $f(M)\, g(\xi P M) = \gamma$. However, as P decreases, the system bifurcates at $P = v/u$, and the solution behind the front changes to the unique off-axes steady state $n = n_s$, $m = m_s$; this bifurcation corresponds to a transcritical bifurcation of the kinetics. Here u and v are the unique roots of $f(u)\, g(v) - 1 = f(u)\, g(\xi v) - \gamma = 0$, so that $n_s = (v - Pu)/(1 - P)$ and $m_s = (u - v)/(1 - P)$. There are no other bifurcations provided $P > 0$, and in fact this critical value of $P = v/u$ is negative for some values of ξ and γ.

In this paper, we consider the much richer bifurcation structure of (2) when P decreases below zero. This is a rather unrealistic parameter regime biologically, and our results are of mathematical interest only. However, they illustrate a novel type of behaviour for reaction–diffusion systems, namely irregular spatiotemporal oscillations when the diffusion coefficients are equal. Moreover initial conditions of the form of a local perturbation of an unstable equilibrium are widespread in biological applications of reaction–diffusion models [38]. We begin by considering the bifurcation structure of the diffusionless equations. For P just below v/u, (n_s, m_s) is a stable node in this system. However, as P decreases, the equilibrium may become a stable focus, depending on the other parameters. If so, there may then be a Hopf bifurcation at some negative value $P = P_{\text{crit}}$, again depending on the other parameters. If such a P_{crit} does exist, then for $P < P_{\text{crit}}$, (n_s, m_s) remains an unstable focus. Since the region $n \geq 0$, $m \geq 0$, $n + Pm > 0$, $1 \leq n + m \leq N$ is a confined set in the n–m phase plane, the Poincaré–Bendixson theorem then implies that the diffusionless equations have a limit cycle solution. The parameter domain for the existence of a limit cycle is illustrated in fig. 1, and the underlying analysis is outlined in the Appendix. In the remainder of the paper, we will investigate the behaviour of the reaction–diffusion equations (2) for parameter values such that the kinetics have a limit cycle solution.

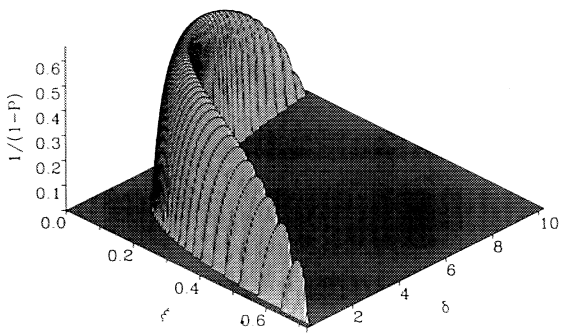

Fig. 1. The parameter domain in which the diffusionless ordinary differential equations corresponding to (2) has a limit cycle solution. The other parameter values are $k = 15$ and $N = 10$. Although we have not proved this analytically, numerical calculation (specifically, integration of the equations both forward and backwards in time for a range of initial conditions) indicates that when a limit cycle exists, it is unique, and thus stable.

3. Reaction–diffusion waves with $P < P_{\text{crit}}$

For $v/u > P > P_{\text{crit}}$, the travelling fronts induced by a local perturbation to the $n = 1, m = 0$ equilibrium leave the system in the steady state

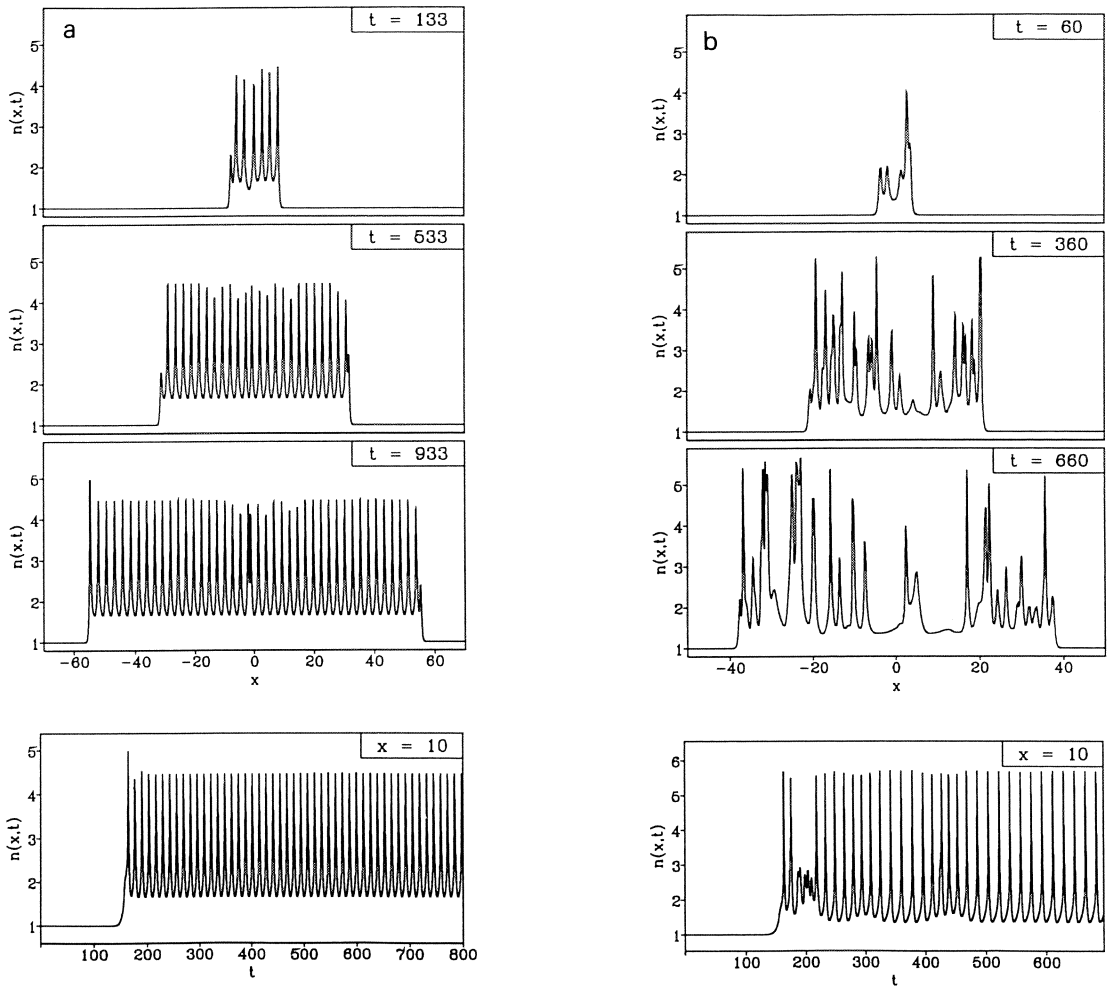

Fig. 2. The two types of behaviour in the wake of the travelling front with $P < P_{crit}$: (a) regular and (b) irregular spatiotemporal oscillations. In both cases, we plot the solutions for $n(x,t)$ of (2) as a function of space x at three times t, and as a function of t at $x = 10$. The solutions for $m(x,t)$ are qualitatively similar. The solution is initially in the homogeneous steady state $n = 1$, $m = 0$, and small random perturbations are applied to this steady state on $-2 \leq x \leq 2$ at $t = 0$. The parameter values are (a) $P = -2$ and (b) $P = -3$, with $\xi = 0.45$, $\gamma = 2$, $k = 15$, $N = 10$ and $D = 0.01$ in both cases. The value of D is essentially irrelevant, since changing D corresponds simply to a rescaling of x. In irregular cases such as (b), there are persistent irregularities in the oscillations (see fig. 3). The qualitative forms of the solutions are not at all sensitive to the details of the initial localised perturbation: in particular, the initial conditions $n = m = 0$ for $|x| > 2$ and $n = n_s$, $m = m_s$ for $|x| < 2$ also give irregular behaviour in (b).

(n_s, m_s) behind the front. It is therefore of little surprise that as P decreases through P_{crit}, so that (n_s, m_s) becomes unstable in the diffusionless system, the reaction–diffusion solutions also bifurcate. Numerical solutions of (2) for $P < P_{crit}$ show that behind the travelling front, whose speed a still remains independent of P, the system exhibits either periodic spatiotemporal oscillations, or is both spatially and temporally irregular (figs. 2 and 3). In contrast to what one might expect intuitively, there is not a simple change from regular to irregular oscillations as P ($< P_{crit}$) is decreased; rather, our numerical solutions suggest that there are a series of intervals of P corresponding to regular and irregular behaviour. When periodic oscillations oc-

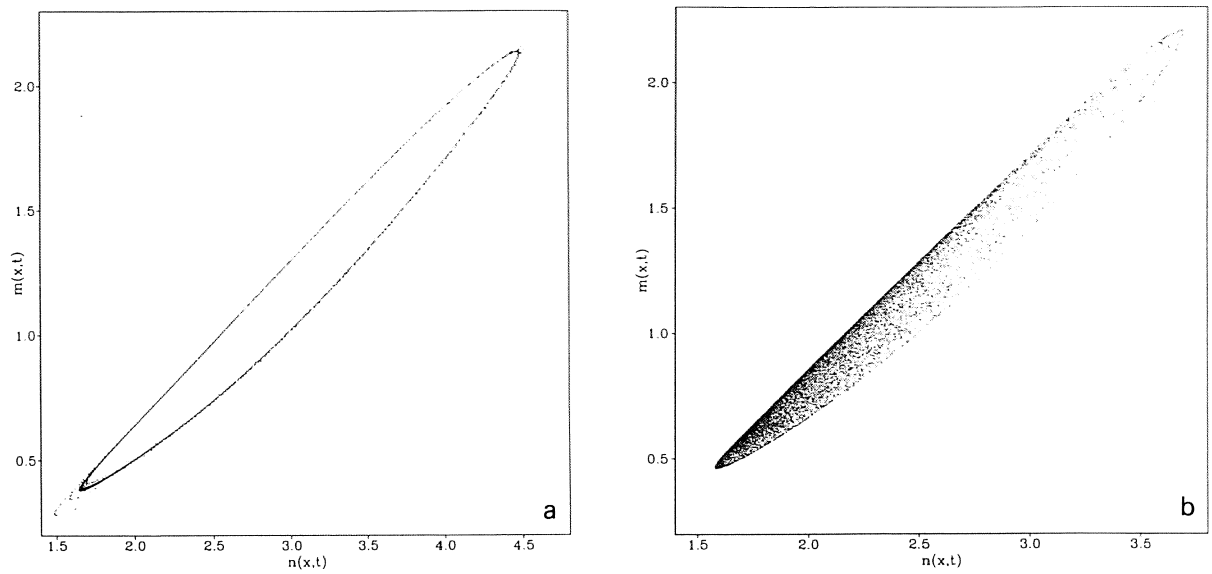

Fig. 3. An alternative visualisation of the solution of (2) following a small, localised perturbation to the steady state $n = m = 0$. We mark the values of n and m at 150 equally spaced times, in each case at every other node in the space mesh that lies behind the travelling front. The solutions in (a) and (b) correspond to regular and irregular spatiotemporal oscillations respectively. The parameter values are $\xi = 0.45$, $\gamma = 2$, $k = 15$, $N = 10$, $D = 0.01$, with (a) $P = -2$ and (b) $P = -1.5$, and with integration up to a maximum time of (a) 1800 and (b) 3000.

cur, these do not move with the travelling front – in fact, the peaks move in the opposite direction to the front. To further confirm that these oscillations do not arise from a bifurcation of the travelling front solution, we investigated the travelling wave ordinary differential equations which govern solutions of the form $n(x,t) = \hat{n}(t + x/a)$, $m(x,t) = \hat{m}(t + x/a)$. Dropping the hats for notational simplicity, this gives the following fourth order system of ordinary differential equations:

$$n' = \frac{D}{a^2}n'' + n[f(n+m)g(n+Pm) - 1], \quad (3a)$$

$$m' = \frac{D}{a^2}m'' + m[f(n+m)g(\xi n + \xi P m) - \gamma]; \quad (3b)$$

recall that $a = 2\sqrt{D[g(\xi) - \gamma]}$. For $P > P_{\text{crit}}$, these equations provide a very good approximation to the full partial differential equation solutions. However, analytical investigation of the local behaviour near the steady state (n_s, m_s), and numerical investigation of the global flow, both fail to show any bifurcation of (3) at $P = P_{\text{crit}}$. Moreover, numerical solutions suggest that in the phase space of (3) there is a heteroclinic connection between $n = 1$, $m = 0$ and $n = n_s$, $m = m_s$ for all values of $P < v/u$. We concluded from this that the travelling front changes continuously as P decreases through P_{crit}, but that the spatially homogeneous equilibrium that the front leaves behind changes stability, and is thus driven unstable by perturbations caused simply by the passage of the front itself. The nature of these perturbations will be discussed explicitly in the next section. This sequence of events is indicated clearly in numerical solutions of (2) with P just below P_{crit}, as illustrated in fig. 4.

To investigate further the solution behind the front, we examined the travelling wave equations (3) for more general wave speeds, c say,

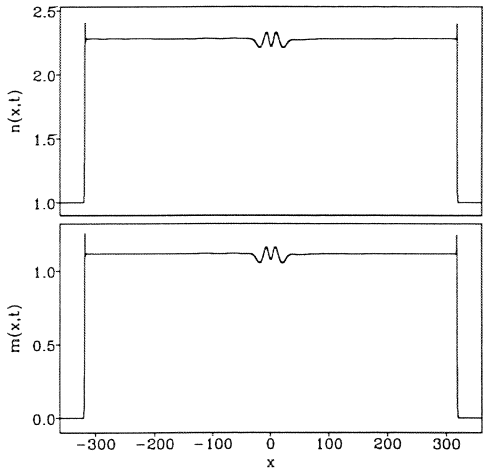

Fig. 4. A typical solution of (2) for P just below P_{crit}. The steady state $n = n_s$, $m = m_s$ is driven unstable by perturbations induced by the passage of the travelling front. However, the solution remains very close to (n_s, m_s) for a considerable distance behind the front, since this steady state is only just unstable. The parameter values are $P = -1.4$, $\xi = 0.45$, $\gamma = 2$, $k = 15$, $N = 10$ and $D = 0.01$; for these parameter values, $P_{crit} \approx -1.3975$. The solution is plotted at $t = 6000$ following a small perturbation of the $n = 1$, $m = 0$ steady state near the origin at $t = 0$.

rather than the particular travelling front speed a. We are considering values of P such that the diffusionless system has a periodic solution, and for kinetics of this form, the travelling wave equations have been studied in detail by a number of authors, in particular Kopell and Howard [39] and Maginu [40]. These authors have shown that the travelling wave equations have a periodic solution for sufficiently large c, arising via a Hopf bifurcation, and that as $c \to \infty$, this periodic solution approaches the periodic solution of the diffusionless system, uniformly in t. Our particular system is

$$n' = \frac{D}{c^2}n'' + n[f(n+m)g(n+Pm) - 1], \quad (4a)$$

$$m' = \frac{D}{c^2}m'' + m[f(n+m)g(\xi n + \xi P m) - \gamma], \quad (4b)$$

and we denote by $\Lambda_1 \pm i\Lambda_2$ the eigenvalues of the diffusionless system at (n_s, m_s) $(\Lambda_1, \Lambda_2 > 0)$. Although the expressions are algebraically cumbersome, we can derive analytical expressions for Λ_1 and Λ_2. It is straightforward to show that the steady state (n_s, m_s) of (4) has a Hopf bifurcation at $c = \Lambda_2\sqrt{D/\Lambda_1} \equiv c_{crit}$. Numerical calculations indicate that a periodic solution exists for all $c > c_{crit}$, which is in keeping with the results of Kopell and Howard [39] and Maginu [40]. For all realistic parameter values the speed of the travelling front a is less than c_{crit}, usually by an order of magnitude.

4. Oscillatory behaviour behind the front

For values of P for which the reaction–diffusion solutions exhibit spatiotemporal oscillations behind the travelling front, numerical calculations show that these oscillations are very well approximated by the periodic solution of (4), for one particular c, c_{obs} say. The oscillatory plane waves move away from the travelling front with speed c_{obs}, and of course the ratio of spatial to temporal periods is also equal to c_{obs}. Since these oscillations are induced by the instability of the homogeneous steady state (n_s, m_s), it is natural to consider whether small random perturbations of this steady state give rise to such spatiotemporal oscillations. Numerical solutions show that this is not so, and that rather the reaction–diffusion system evolves to spatially homogeneous oscillations, which are periodic in time, and correspond to the periodic solution of the diffusionless system. This is not suprising, since the fastest growing Fourier mode at (n_s, m_s) is the spatially homogeneous mode. These homogeneous oscillations are simply the periodic solution of the diffusionless system.

This suggests that the particular perturbation that is applied to the steady state (n_s, m_s) by the passage of the travelling front causes the perturbation to grow into a periodic plane wave with period ratio c_{obs}. We were able to confirm

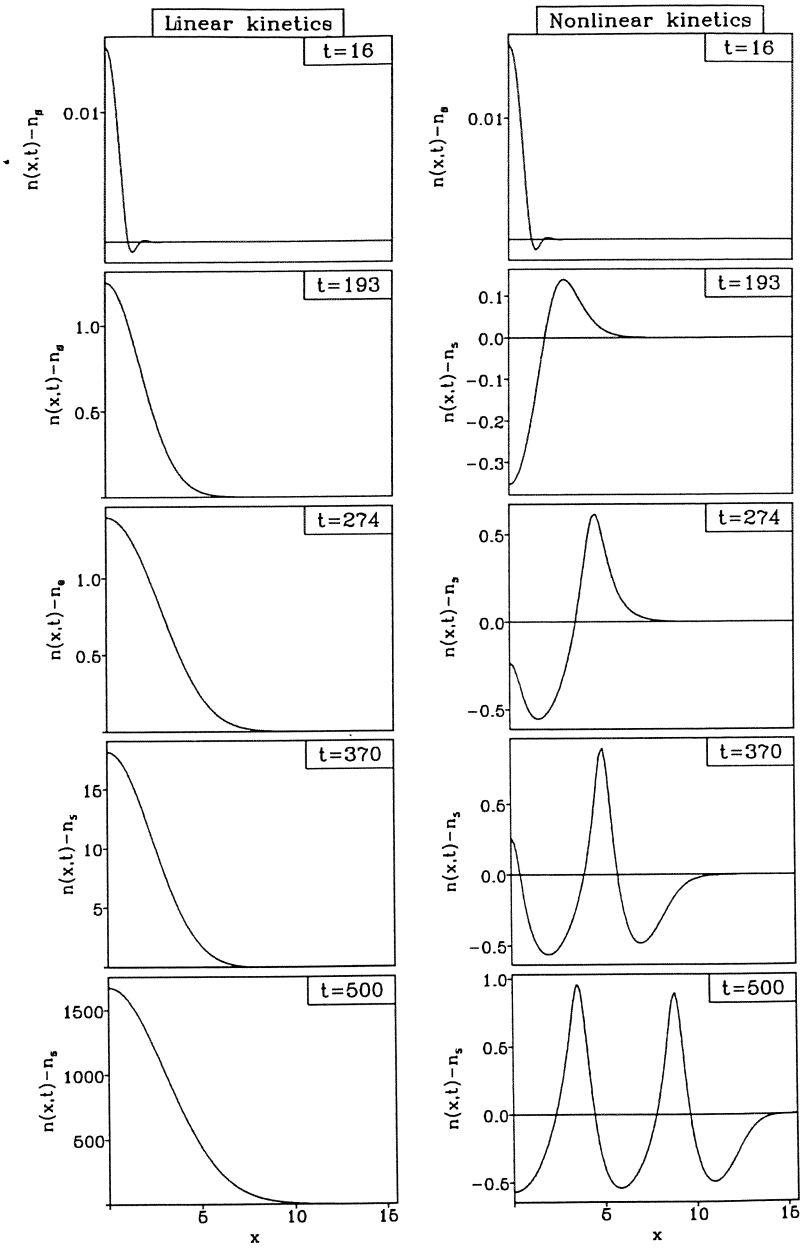

Fig. 5. Comparison of the linearised and full nonlinear model solutions, following an induced perturbation. These solutions show that the evolution of periodic plane waves is a strictly nonlinear phenomenon. We plot the solutions for $n(x,t)$ of the full model (2), and of the corresponding equations when linearised about (n_s, m_s). The solutions for $m(x,t)$ are qualitatively similar. The initial conditions are $(n,m) = (n_s,m_s) + 0.01(n_r \pm n_i, m_r \pm m_i)\, e^{(-\lambda_1 \pm i\lambda_2)x/a}$, where $-\lambda_1 \pm i\lambda_2$ are the eigenvalues of (3) at (n_s,m_s), and $(n_r \pm n_i, m_r \pm m_i)$ are the corresponding eigenvectors. This is the perturbation induced by the rear of the travelling front, and in the full nonlinear model it induces oscillatory plane waves with the same spatial to temporal period ratio as in the travelling front solutions (see fig. 7, below). However, in the linearised equations, spatiotemporal oscillations do not develop. In fact, the direction and rate of oscillation of the perturbation are not crucial in determining the solution in the full model, and the resulting behaviour depends mainly on the real part of the eigenvalue, λ_1. The parameter values are $P = -1.5$, $\xi = 0.45$, $\gamma = 2$, $D = 0.01$, $k = 15$ and $N = 10$, which gives $a \approx 0.047$, $\lambda_1 \approx 0.13$ and $\lambda_2 \approx 0.23$.

this conclusion by a simple numerical test. The form of the rear of the travelling front, moving to the left, say, as it approaches (n_s, m_s) is simply $e^{(-\lambda_1 \pm i\lambda_2)(t+x/a)}$, where $-\lambda_1 \pm i\lambda_2$ are the two eigenvalues of (3) at (n_s, m_s) with negative real part. (It is straightforward to show that the four eigenvalues will be in two complex conjugate pairs, with one pair having positive real part and one having negative real part). Here λ_1 and λ_2 are positive, and are known analytically. We solved the reaction–diffusion system (2) numerically on $0 \leq x \leq L$, with initial conditions of the form $(n, m) = (n_s, m_s) + \epsilon(n_r \pm in_i, m_r \pm im_i)\, e^{(-\lambda_1 \pm i\lambda_2)x/a}$. Here $\epsilon \ll 1$, $L \gg 1/\lambda_1$, and $(n_r \pm in_i, m_r \pm im_i)$ are the (complex conjugate) eigenvectors of (3) corresponding to the eigenvalues $-\lambda_1 \pm i\lambda_2$. We found that the system did indeed evolve to periodic plane waves, moving with the same speed c_{obs} as was found in the travelling front solutions with the same parameter values (see fig. 5, below). These results were independent of ϵ and L, and of whether the boundary conditions were of Neumann or Dirichlet type.

One of the best studied aspects of reaction–diffusion systems is diffusion driven instability, in which a steady state that is stable in the diffusionless system is driven unstable by the diffusion terms [1,2]. In this process, the system typically evolves to a stationary, spatially oscillating state which is a solution of the nonlinear steady state differential equations. However, in a wide variety of cases it has been found that, even quite far from the primary bifurcation point, the shape of this steady state solution is well approximated by the solutions of the linear partial differential equation system governing small oscillations about the initial homogeneous steady state [41,42]; these linear equations can usually be solved analytically.

With this in mind, it was natural to consider whether insight could be gained into the observed periodic plane waves by investigating the reaction–diffusion system with the kinetics linearized about (n_s, m_s). However, our analytical attempts proved fruitless, and comparison of the linear and nonlinear systems following an imposed perturbation to (n_s, m_s) revealed that the evolution of the periodic plane waves is indeed a truly nonlinear phenomenon (fig. 5). This is in sharp contrast to the case of diffusion driven instability.

We have been unable to determine an exact expression for c_{obs} in terms of the model parameters. However, an approximate expression can be derived by the following simple argument. The travelling front moves with speed a, and generates in its wake periodic plane waves which move away from the front with speed c_{obs}. Now the perturbations arising from the travelling front generate a peak in the periodic plane wave at regular time intervals, τ say. Therefore, during the time interval between the generation of successive peaks, the travelling front and the last peak to be generated will increase their separation by a distance $\tau(a + c_{obs})$. This increase in separation will be approximately equal to the spatial period of the periodic plane waves, which is $c_{obs}T(c_{obs})$, where $T(c)$ is the period of the periodic solution of (4) for $c > c_{crit}$. The equality is only approximate because the peak separation may change as the waves evolve. It remains to estimate τ. Consider small perturbations to the steady state (n_s, m_s) of the form $(n, m) = (n_s, m_s) + (\tilde{n}, \tilde{m})\, e^{ikx+wt}$, $(|\tilde{n}|, |\tilde{m}| \ll 1)$. Substituting these solution forms into (2) shows that

$$(\omega + Dk^2)(\tilde{n}, \tilde{m}) = A \cdot (\tilde{n}, \tilde{m}) + \mathcal{O}\left((\tilde{n} + \tilde{m})^2\right), \quad (5)$$

where A is the stability matrix of the diffusionless system at (n_s, m_s). Therefore to leading order, $\omega = \Lambda_1 - Dk^2 \pm i\Lambda_2$, where, as previously, $\Lambda_1 \pm i\Lambda_2$ are the eigenvalues of A. Therefore all unstable modes oscillate with the same frequency $\Lambda_2/2\pi$, suggesting that $\tau \approx 2\pi/\Lambda_2$. Thus we expect that

$$T(c_{obs}) \approx (2\pi/\Lambda_2)(1 + a/c_{obs}). \quad (6)$$

Table 1
The speed c_{obs} of plane waves induced behind the travelling front in solutions of (2), following a localised perturbation of the $n = 1$, $m = 0$ steady state. The observed plane wave speed is compared with the solution of eq. (6), showing that this equation provides a semi-quantitative approximation to c_{obs} . We also compare the values of the two sides of this equation, to show that they agree reasonably well.

ξ	γ	P	c_{obs}	Solution of (6)	RHS/LHS of (6)
0.45	2.0	−1.5	0.38	0.42	1.01
0.45	2.0	−1.6	0.31	0.31	1.02
0.45	2.0	−1.65	0.29	0.31	1.06
0.45	2.0	−2.0	0.21	0.30	1.17
0.40	2.0	−1.0	1.66	0.90	0.94
0.60	1.5	−2.0	1.40	0.25	0.98
0.25	3.0	−0.9	0.58	0.66	1.02
0.25	3.0	−0.6	1.35	1.61	1.02
0.30	2.2	−2.5	0.81	0.65	0.97

Here Λ_2 is known analytically as a function of the model parameters, but $T(\cdot)$ can only be determined numerically. Such numerical calculations show that for the values of c_{obs} found in the reaction–diffusion solutions, the two sides of (6) agree reasonably well (table 1).

$T(c_{crit}) = 2\pi/\Lambda_2$, since the eigenvalues through which the Hopf bifurcation of (4) occurs at $c = c_{crit}$ have imaginary part Λ_2. Moreover, as $c \to \infty$, the results of Kopell and Howard [39] and Maginu [40] imply that $T(c)$ approaches the period of the limit cycle in the diffusionless system. Numerical calculations suggest that this period is always greater than $2\pi/\Lambda_2$, and that $T(c)$ increases monotonically between these two values, except for a small non-monotonic variation close to c_{crit} (fig. 6) . Conversely, the right hand side of (6) decreases monotonically, tending to $2\pi/\Lambda_2$ as $c_{obs} \to \infty$. Therefore, if we consider (6) as an equation for c_{obs} , it has exactly one root on (c_{crit}, ∞) (see fig. 6) . As expected, this root does not give a particularly good quantitative approximation to c_{obs} , but it does provide a qualitative estimate which reflects the variations in c_{obs} with the model parameters (table 1).

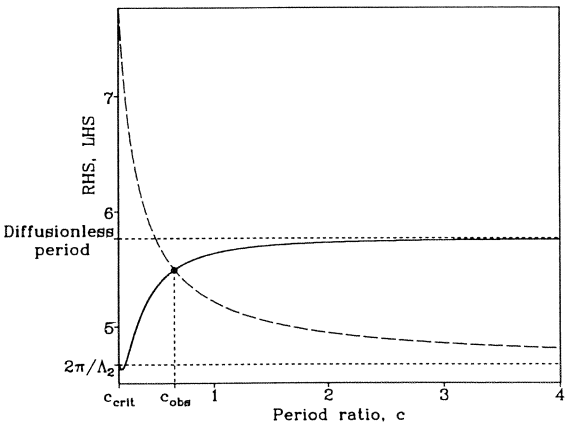

Fig. 6. Typical forms of the right hand side ------- and left hand side ——— of (6) . As $c \to \infty$, $T(c)$ tends towards the period of the limit cycle solution of the diffusionless system, while the right hand side of (6) tends towards $T(c_{crit})$. The intersection of these two curves gives a semi-quantitative approximation to c_{obs} , the plane wave period ratio induced by the passage of the travelling front (see table 1).

5. The origin of irregularities

We now use our understanding of the case of regular spatiotemporal oscillations behind the travelling front to investigate the parameter regions in which the oscillations are irregular in this wake region. The key to understanding the origin of this irregularity lies in the stability of

periodic travelling waves as solutions of the full partial differential equation system. This issue was discussed in detail in the seminal paper of Kopell and Howard [39]. They showed that as a solution of a reaction–diffusion system whose kinetics have a limit cycle, the periodic solution of the corresponding travelling wave equations is unstable close to the Hopf bifurcation in c, but at least in the case of equal diffusivities, is stable for sufficiently large c. For a particularly simple type of kinetics known as a λ–ω system, Kopell and Howard [39] showed further that a necessary and sufficient condition for stability is that c is larger than a critical value, which they obtained analytically. The corresponding result for more general kinetics remains unsolved, although there have been a number of subsequent advances [40,43,44].

Our kinetics are not of λ–ω type, and we have been unable to gain any analytical insight into the stability of the periodic plane waves as a solution of the reaction–diffusion system. However, stability can be investigated numerically. To do this, we obtained a numerical approximation to the periodic solution for various values of c using the continuation package AUTO [45,46]. We then applied small random perturbations to this solution, and used it as the initial condition in a numerical solution of the full reaction–diffusion system on a small space domain, of length a whole number of periods (typically 4 or 5). This numerical investigation suggested that, as for λ–ω systems, there was a critical value of c, c_{stab} say, such that $c > c_{\text{stab}}$ was a necessary and sufficient condition for stability. However, it should be remembered that the restriction on the domain size precludes observation of instability to large scale perturbations.

Comparison of c_{stab}, c_{obs} and numerical solutions of the partial differential equations suggests that for $P < P_{\text{crit}}$, the cases of regular and irregular spatiotemporal oscillations are distinguished by $c_{\text{obs}} > c_{\text{stab}}$ and $c_{\text{obs}} < c_{\text{stab}}$ respectively; of course, this conclusion can only be as precise as our approximation for c_{obs} . That is, the travelling front induces periodic plane waves behind the front, and these either persist or evolve into spatiotemporal irregularities, depending on their stability. Although it is possible that unstable waves could evolve to some other regular behaviour, such as higher speed periodic plane waves, we have no evidence that this ever occurs. To summarise, our results suggest that the full sequence of events by which the irregular wakes arise is as follows. Behind the travelling front, the solution approaches the steady state (n_s, m_s). However, this steady state is unstable in the diffusionless system, and the particular perturbation induced by the passage of the front causes periodic plane waves to evolve from the steady state. These plane waves

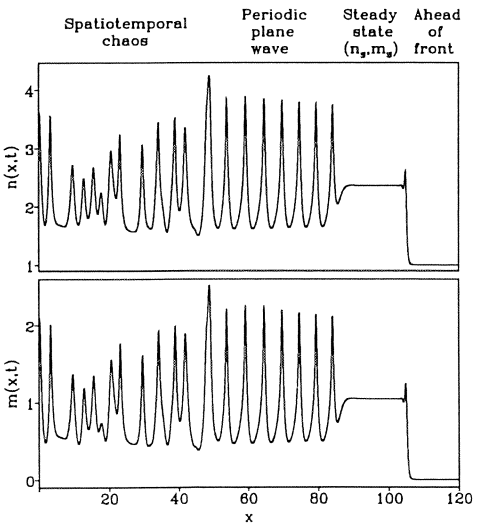

Fig. 7. A solution of (2) for parameter values such that c_{obs} is just below c_{stab} and P is just below P_{crit} . This means that the steady state (n_s, m_s) and the periodic plane waves induced by the travelling front are both just unstable as solutions of the full reaction–diffusion system. This solution therefore illustrates the full sequence of events by which the irregular wakes arise. Immediately behind the travelling front, the solution is close to the steady state (n_s, m_s). However, this is unstable, and the passage of the front induces periodic plane waves. These plane waves are themselves unstable, giving rise to irregular oscillations. The parameter values are $P = -1.5$, $\xi = 0.45$, $\gamma = 2$, $k = 15$, $N = 10$ and $D = 0.01$, and the solution is illustrated at $t = 1885$ for $x > 0$ only. For these parameters $P_{\text{crit}} \approx -1.3975$, $c_{\text{stab}} \approx 0.85$, and $c_{\text{obs}} \approx 0.4$.

move in the opposite direction from the travelling front with speed c_{obs}, which is determined by the particular way in which the rear of the front approaches (n_s, m_s). However, these periodic plane waves are themselves unstable as solutions of the reaction–diffusion system, and their destabilization gives rise to spatiotemporal irregularites. The full sequence of events can be seen very clearly in solutions for parameters such that c_{obs} is a little below c_{stab} and also P is close to P_{crit}, as illustrated in fig. 7. More generally, the instabilities of (n_s, m_s) and the periodic plane waves are so strong that these transient states are too short-lived to be observed (see fig. 2b); however, we speculate that the sequence of events is essentially the same.

6. Conclusions

Reaction–diffusion models have been highly successful in exhibiting many types of experimentally observed nonlinear phenomena, but spatiotemporal irregularities and chaos are a notable exception. We have investigated in detail one particular system of two coupled reaction–diffusion equations, and have shown how irregular spatiotemporal oscillations can develop behind a travelling front. This is a new mechanism by which irregular behaviour can arise naturally in reaction–diffusion systems, and does not require unequal diffusivities. A crucial outstanding question concerns the generality of this mechanism for the generation of spatiotemporal irregularities in reaction–diffusion systems. As a small, preliminary step towards answering this question, we have solved (2) for a number of other functional forms for f and g, in each case for a wide range of parameter values. Our solutions were always qualitatively similar to those for the particular functional forms considered previously, which raises the possibility that our results may generalise to a much wider class of reaction–diffusion systems.

7. Acknowledgements

I am extremely grateful to Dr Alan Champneys (School of Mathematics, University of Bath) for help with the AUTO package. Thanks also to Professor Robert May for helpful comments, and to Dr Philip Maini and Dr Wendy Brandts (Centre for Mathematical Biology, Oxford) for advice and support. This work was supported in part by a Junior Research Fellowship at Merton College, Oxford.

Appendix

We now outline the calculation of the stability of the steady state (n_s, m_s), on which fig. 1 is based. The stability matrix at (n_s, m_s) is given by

$$A = \begin{pmatrix} n_s[f'(u)\,g(v) + f(u)\,g'(v)] & n_s[f'(u)\,g(v) + Pf(u)\,g'(v)] \\ m_s[f'(u)\,g(\xi v) + \xi f(u)\,g'(\xi v)] & m_s[f'(u)\,g(\xi v) + P\xi f(u)\,g'(\xi v)] \end{pmatrix}, \tag{7}$$

where as previously $u = n_s + m_s$ and $v = n_s + Pm_s$. Recall that u and v are independent of the parameter P, being solutions of $f(u)\,g(v) - 1 = f(u)\,g(\xi v) - \gamma = 0$. For the forms of f and g given in the main body of the paper, straightforward analysis shows that

$$u = N - \gamma(N-1)(1-\xi)/[k(1-\xi\gamma)], \tag{8a}$$

$$v = \delta/[(k-1)(1-\xi\gamma)]. \tag{8b}$$

Considerable algebraic manipulation then yields the following expressions for the determinant and trace of A:

$$\det(\mathrm{A}) = (1-\xi\gamma)g(v)^2 g(\xi v)\,(u-v)^2 \frac{k}{(k-1)(N-1)}\left(\frac{u}{u-v} - \frac{1}{(1-P)}\right),$$

$$\begin{aligned}\mathrm{tr}(\mathrm{A}) &= (k-1)u\left(\frac{1-\gamma\xi}{1-\xi}\right)\\ &\quad\times\left[(1-v/u)\xi\gamma^2 - 1 - \frac{k}{(k-1)(N-1)}\right.\\ &\quad\left.+(1-v/u)\left(1-\xi\gamma^2 - \frac{k(\gamma-1)}{(k-1)(N-1)}\right)\frac{1}{1-P}\right].\end{aligned} \tag{9}$$

The crucial aspect of these expressions is that for given values of the other parameters, both $\det(\mathrm{A})$ and $\mathrm{tr}(\mathrm{A})$ vary linearly with $1/(1-P)$. Now we are considering only the parameter domain in which travelling fronts exist, that is $g(\xi) > \gamma$, which implies that $\xi\gamma < 1 - (\gamma-1)/(k-1) < 1$. Therefore $\det(\mathrm{A})$ decreases as P increases, and is zero at the bifurcation value $P = v/u$, so that $\det(\mathrm{A}) > 0$ whenever (n_s, m_s) lies in the first quadrant.

To consider the possibility of Hopf bifurcations, we must investigate $\mathrm{tr}(\mathrm{A})$, which can either increase or decrease with P, depending on the other parameters. Since $\mathrm{tr}(\mathrm{A})$ is obviously negative when $P > 0$, there will be a Hopf bifurcation for some value of P if and only if $\mathrm{tr}(\mathrm{A})$ decreases with P and also is positive at $P = -\infty$. Since $\det(\mathrm{A}) > 0$, (n_s, m_s) will then be unstable for all P below this bifurcation value. Rearranging (9) shows that $\mathrm{tr}(\mathrm{A}) > 0$ if and only if

$$\begin{aligned}&\left(\frac{\gamma^2[1-1/(1-P)]}{1+k/[(k-1)(N-1)]}\right)\xi + \left(\frac{1-(\gamma-1)k/[(k-1)(N-1)]}{(1-P)(1+k/[(k-1)(N-1)])}\right)\\ &> \left(\frac{(k/\gamma)\cdot N/(N-1)-1}{k\cdot N/(N-1)-1} - \xi\right)\Big/\left(\frac{(k/\gamma)-1}{k-1} - \xi\right).\end{aligned} \tag{10}$$

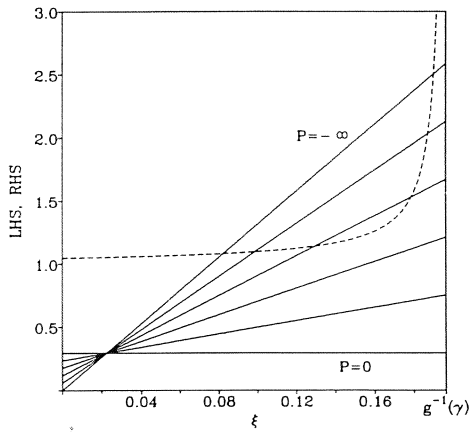

Fig. 8. The right hand side ------- and left hand side ——————— of eq. (10) as functions of ξ. The left hand side is shown for a range of values of P. The other parameter values are $\gamma = 4$, $N = 6$ and $k = 15$, but the qualitative features are the same for all values of these parameters, within the constraints discussed in the text. In particular, for each set of values of P, γ, k and N, (10) holds either for no values of ξ or for a subinterval of $0 < \xi < g^{-1}(\gamma)$.

The qualitative forms of the two sides of this inequality as functions of ξ are illustrated in fig. 8, which shows that for given values of the other parameters, the steady state (n_s, m_s) is either stable for all values of ξ, or is unstable when ξ lies on a subinterval of $0 < \xi < (k/\gamma - 1)/(k - 1) = g^{-1}(\gamma)$. This subinterval becomes larger as P decreases to $-\infty$, giving a parameter domain for the existence of a limit cycle of the form illustrated in fig. 1. Whatever direction this domain is entered, the limit cycle arises via a Hopf bifurcation.

References

[1] A.M. Turing, Phil. Trans. R. Soc. 237 (1952) 37.
[2] J.D. Murray, J. Theor. Biol. 88 (1981) 161.
[3] H. Meinhart, Models of Biological Pattern Formation (Academic Press, London, 1982).
[4] J.A. Sherratt and J.D. Murray, J. Math. Biol. 29 (1991) 389.
[5] N. Kopell and L.N. Howard, Science 180 (1973) 1171.
[6] S.R. Dunbar, J. Math. Biol. 17 (1983) 11.
[7] S.C. Müller, T. Plesser and B. Hess, Physica D 24 (1987) 71.
[8] J.M. Greenberg, SIAM J. Appl. Math. 39 (1980) 301.
[9] P.S. Hagan, SIAM J. Appl. Math. 42 (1982)762.
[10] I. Prigogine and R. Lefever, J. Chem. Phys. 48 (1968) 1695.
[11] Y. Kuramoto, Prog. Theor. Phys. S64 (1978) 346.
[12] P.J. Nandapurkar, V. Hlavacek and P. Van Rompay, Chem. Eng. Sci. 41 (1986) 2747.
[13] A.B. Rovinsky, J. Phys. Chem. 91 (1987) 5113.
[14] S. Wolfram, Nature 311 (1984) 419.
[15] M.P. Hassell, H.N. Comins and R.M. May, Nature 353 (1991) 255.
[16] K. Satoh, J. Phys. Soc. Jap. 58 (1989) 3842.
[17] M.A. Nowak and R.M. May, Nature, in press.
[18] H. Hartman and P. Tamayo, Physica D 45 (1990) 293.
[19] Y. Oono and M. Kohmoto, Phys. Rev. Lett. 55 (1985) 2927.
[20] Y. Oono and C. Yeung, J. Stat. Phys. 48 (1987) 593.
[21] J.B. Salem and S. Wolfram, in: Theory and Applications of Cellular Automata, ed. S. Wolfram (World Scientific, Singapore, 1986) p. 362.
[22] X.J. Wang and G. Nicolis, Physica D 26 (1987) 140.
[23] I. Schreiber and M. Marek, Physica D 5 (1982) 258.
[24] J.C. Alexander, in: Lecture Notes on Biomathematics, No. 66, ed. H.G. Othmer (Springer, Berlin, 1986) p. 208.
[25] O.E. Rössler, Z. Naturforsch. A 31 (1976) 1168.
[26] H. Fujisaka and T. Yamada, Prog. Theor. Phys. 69 (1983) 32.
[27] J.A. Sherratt and J.D. Murray, Proc. R. Soc. London B 241 (1990) 29.
[28] J.A. Sherratt and J.D. Murray, Comments Theor. Biol. 2 (1992) 315.
[29] J.A. Sherratt and J.D. Murray, Cell Transplantation 1 (1992) 365.
[30] R.A. Weinberg, in: Oncogenes and the Molecular Origins of Cancer, ed. R.A. Weinberg (Cold Spring Harbor Laboratory Press, 1989) p. 45.
[31] R.A. Weinberg, Science 254 (1991) 1138.
[32] T.E. Wheldon, J. Theor. Biol. 53 (1975) 421.
[33] J.A. Sherratt and M.A. Nowak, Proc. R. Soc. B 248 (1992) 261.
[34] C. Naftzger and A.N. Houghton, Curr. Op. Oncol. 3 (1991) 75.
[35] W. Alt, J. Math. Biol. 24 (1980) 691.
[36] J.D. Murray, P.K. Maini and R.T. Tranquillo, Phys. Rep. 171 (1988) 59.
[37] J.A. Sherratt, SIAM J. Appl. Math., in press.
[38] J.D. Murray, Mathematical Biology (Springer, Berlin, 1989).
[39] N. Kopell and L.N. Howard, Stud. Appl. Math. 52 (1973) 291.
[40] K. Maginu, J. Diff. Eqs. 39 (1981) 73.
[41] J.D. Murray, J. Theor. Biol. 98 (1982) 143.
[42] D. Benson, J.A. Sherratt and P.K. Maini, Bull. Math. Biol. 55 (1993) 365.
[43] D. Cope, SIAM J. Appl. Math. 38 (1980) 457.
[44] K. Maginu, SIAM J. Appl. Math. 45 (1985) 750.
[45] E. Doedel, Cong. Numer. 30 (1981) 265.
[46] E. Doedel and J.P. Kernevez, Applied Mathematics Technical Report, California Institute of Technology (1986).